Asian Journal of Chemistry; Vol. 37, No. 12 (2025), 3025-3035
ASIAN JOURNAL OF CHEMISTRY
https://doi.org/10.14233/ajchem.2025.34665

Synthesis, Characterization and *in silico* Evaluations of Novel Chalcone Derivatives Containing Oxindole Ring

ATIF HUSAIN[1], WASEEM AHMAD ANSARI[1,2], ABDUL RAHMAN KHAN[1], MOHD ARSH KHAN[1] and MALIK NASIBULLAH[1,*]

[1]Department of Chemistry, Integral University, Lucknow-226026, India
[2]Department of Biotechnology, Era's Medical College & Hospital, Era University, Lucknow-226003, India

*Corresponding author: E-mail: malik@iul.ac.in

Received: 8 August 2025 *Accepted*: 4 October 2025 *Published online*: 30 November 2025 AJC-22191

In this study, a new series of chalcone derivatives containing an oxindole moiety to evaluate their physico-chemical properties, pharmacokinetic profiles and *in silico* biological potential. The designed derivatives **3a-d** were obtained *via* a condensation reaction between 5-halo-isatin and substituted acetophenones using sodium ethoxide under moderate reaction conditions. The structures of the synthesized chalcone derivatives were confirmed using ^{1}H NMR, ^{13}C NMR and HRMS. The *in silico* evaluations were performed using established database platforms, including SwissADME and admetLAB 3.0, to assess their absorption, distribution, metabolism, excretion and toxicity (ADMET) properties. All the compounds exhibited favourable drug-likeness, low predicted toxicity and compliance with Lipinski's rule of five, suggesting their potential as orally active therapeutic agents. Molecular docking studies were also carried out to assess the binding affinities of compounds **3a-d** against cancer-related target proteins such as PDGFRα (PDB ID: 9GZH) and VEGFR2 (PDB ID: 4ASD). Compounds **3b** and **3d** demonstrated the most promising binding energies (–11.973 and –7.726 kcal/mol, respectively), outperforming the reference drug, sunitinib. The docking results revealed key hydrogen bonding and hydrophobic interactions, offering insights into the stability of the compounds within the active sites of the target proteins.

Keywords: Anticancer activity, Chalcone, Isatin, Oxindole, Molecular docking, Pharmacokinetics, Drug-likeness.

INTRODUCTION

Chalcones are a significant class of compounds, occurring both naturally and synthetically, that have gained considerable attention in medicinal and pharmaceutical chemistry due to their broad spectrum of biological activities, as well as their structural flexibility and diversity [1]. A distinct property of chalcones is their relatively simple yet highly adaptable framework, which can be readily modified through the substitution of specific functional groups to achieve desired molecular properties while retaining their broad range of applications [2,3]. These chalcones also showed the biological significant role in medicinal chemistry therefore it became driving factor for a large group of researchers to synthesize oxindole-chalcone hybrid derivatives [4]. Among the various scaffolds available for constructing novel chalcone derivatives, isatin as a heterocyclic moiety, offers privileged structural and pharmacological attributes [5].

Isatin, an versatile compound, imparts additional rigidity, hydrogen-bond-donating ability and electron withdrawing properties when fused into or attached to chalcone scaffolds [6]. This fusion not only enhances the physico-chemical properties of the molecules but also provides a versatile platform for the design and development of hybrid compounds with improved efficacy and selectivity. Chalcones derived from isatin have been reported to exhibit a wide range of biological activities [7], including antimicrobial [8-10], anticancer [11-13], antioxidant [14], anti-inflammatory [15], antimalarial [16] and antiviral effects [17]. These activities are often attributed to their multimodal mechanisms of action, involving interactions with multiple biological targets such as enzymes, receptors and nucleic acids, supporting their potential in multi-target drug discovery. The combination of the chalcone moiety with the isatin core results in compounds that demonstrate enhanced bioactivity compared to either simple chalcones or isatin-derived chalcones [18]. In addition to their therapeutic potential, these dual pharmacophores often exhibit favourable drug-like properties, such as improved solubility, chemical stability and binding affinity [19].

Isatin-based chalcones combine the structural simplicity and reactivity of chalcones with the pharmacological potential of isatin. This unique fusion offers a valuable platform for the rational design of novel molecules capable of addressing the growing demand for effective agents against resistant pathogens and complex diseases. Remarkably, recent studies have demonstrated that isatin-based chalcones act as effective inhibitors of cancer cell proliferation [20], modulators of oxidative stress [21] and functional antimicrobial agents, even against drug-resistant strains [22].

The global rise in drug resistance and the need for multifunctional therapeutics have further fuelled interest in this scaffold. As a result, isatin-derived chalcones are emerging as a valuable chemotype in medicinal chemistry, with significant potential for future research focused on their synthesis, properties and biological applications in the development of next-generation therapeutics. The oxindole-containing drugs are used in the treatment of various carcinomas after getting FDA approval [23]. Moreover, as per preceding research work it was observed that chalcones are also showed the biological significant role in medicinal chemistry therefore, we decided to synthesise the oxindole-chalcone hybrid derivatives. Not only that, the molecular docking analysis was also conducted for finding their anticancer properties as preliminary investigation. Therefore, docked complexes were expressed the binding affinities among the synthesized oxindole-chalcone as ligands and PDGFRα/VEGFR2 proteins. Owing to PDGFRα/VEGFR2 refers to two related but distinct receptor tyrosine kinases [24] as both receptors play crucial roles in cell growth, survival and blood vessel formation (angiogenesis) and their deregulations is often linked to various diseases, especially cancers.

EXPERIMENTAL

General procedure: Equimolar quantities (2 mmol each) of 5-halo-isatin (**1**) and substituted acetophenone (**2**) were dissolved in absolute ethanol and stirred gently at room temperature [24]. An ethanolic solution of sodium ethoxide was then added dropwise to the reaction mixture under continuous stirring. The mixture was stirred at room temperature for 1-2 h and the progress of the reaction was monitored by TLC using a 7:3 hexane:ethyl acetate solvent system. Upon completion, the reaction mixture was evaporated to dryness to obtain the crude solid product, which was then washed to afford the purified chalcone derivatives (**Scheme-I**).

All required chemicals, including 5-fluoroisatin, 5-chloroisatin, 5-bromoisatin, acetophenone, *o*-methoxyacetophenone, *p*-aminoacetophenone and sodium ethoxide, were procured from Sigma-Aldrich. Solvents such as ethanol, hexane and ethyl acetate were used as received. FT-IR spectra were recorded on an Alpha-II 210966 FT-IR spectrometer over the range of 3500-500 cm^{-1} at the IIRC-CIF facility, Integral University, Lucknow-226026, India.

^{1}H and ^{13}C NMR spectra were obtained on a JEOL JNM-FCZ400S spectrometer operating at 400 MHz for ^{1}H and 100 MHz for ^{13}C using DMSO-d_6 as the solvent. NMR analyses were performed at Babasaheb Bhimrao Ambedkar University, Lucknow-226025, India.

(*Z*)-5-Bromo-3-(2-(2-methoxyphenyl)-2-oxoethylidene)-indolin-2-one (3a): Creamy solid, yield 77%, m.p.: 372.23 ºC; FT-IR (KBr, ν_{max}, cm^{-1}): 3334.58 (NH *str.*), 2957.88 (sp^2-hybridized C-H *str.*), 2669.80 (sp^3-hybridized C-H *str.*), 1711.69 (>C=O) 1634.04 (>C=C<). ^{1}H NMR (400 MHz,

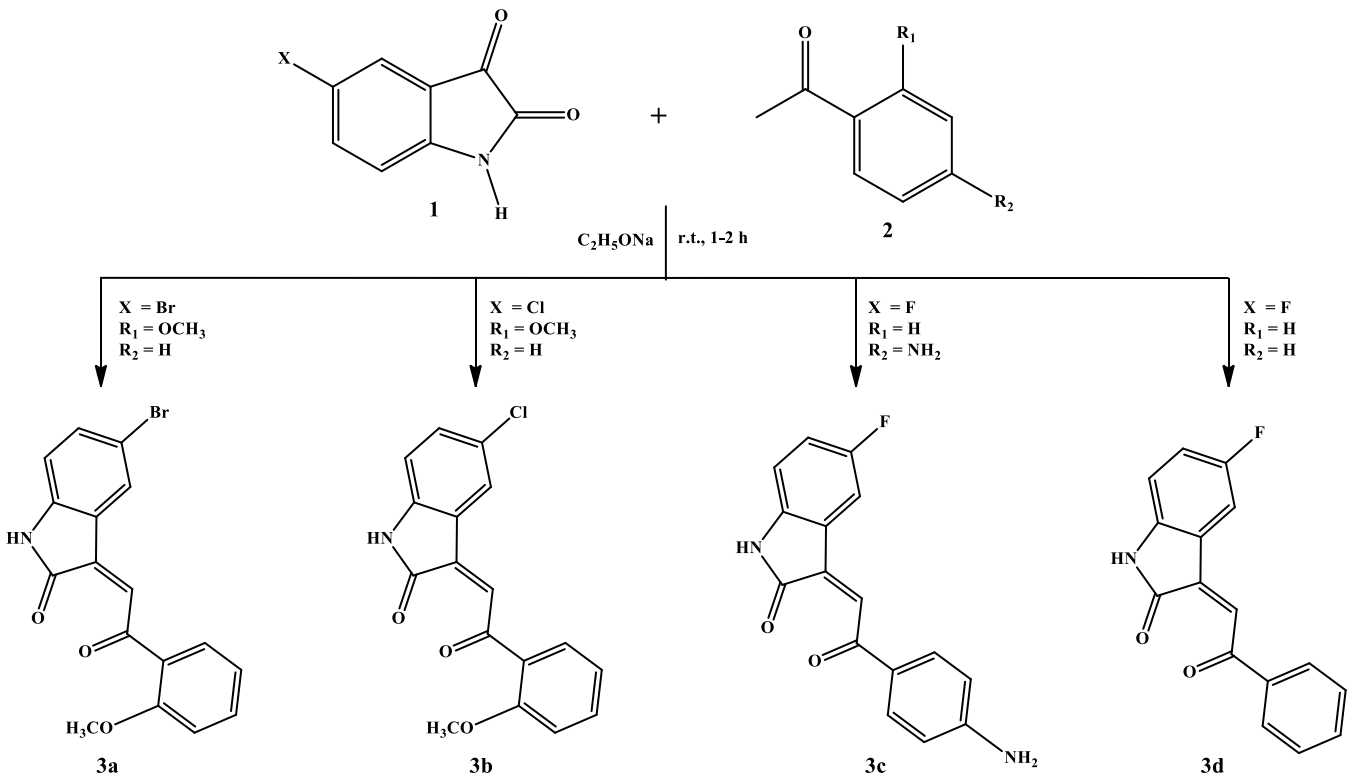

Scheme-I: Schematic overview of the reaction and synthesized derivatives (**3a-d**)

DMSO-d_6, δ ppm): 10.40 (s, 1H, NH), 7.48 (d, J = 8.4 Hz, 1H, ArH), 7.42-7.32 (m, 4H, ArH), 6.78 (d, J = 8.0 Hz, 1H, ArH), 6.76 (d, 1H, ArH), 6.18 (s, 1H, CH), 4.16 (t, 2H, CH_2), 4.12 (s, 2H, CH_2), 3.78-3.30 (m, 3H, OCH_3), 2.49-2.48 (m, 2H, CH_2), 0.89-1.00 (m, minor aliphatic); ^{13}C NMR (100 MHz, DMSO-d_6, δ ppm): 196.341, 177.884, 159.361, 142.337, 137.297, 134.350, 131.485, 129.918, 126.641, 120.522, 119.751, 112.856, 112. 147, 111.380, 72.996, 55.297, 45.844, 40.128, 39.917, 39.711, 39.500, 39.289, 39.083, 38.872. HR-MS: *m/z* found 357.97 for $C_{17}H_{12}BrNO_3^+$.

(*Z*)-5-Chloro-3-(2-(2-methoxyphenyl)-2-oxoethylidene)-indolin-2-one (3b): Creamy solid, yield 75%, m.p.: 342.35 ºC; FT-IR (KBr, ν_{max}, cm^{-1}): 3151.06 (NH *str.*), 2936.08 (sp^2-hybridized C-H *str.*), 2723.14 (sp^3-hybridized C-H *str.*), 1747.36 (>C=O) 1667.37 (>C=C<). ^{1}H NMR (400 MHz, DMSO-d_6, δ ppm): 10.39 (s, NH), 7.48 (m, ArH), 7.41 (m, ArH), 7.37 (m, ArH), 7.36 (m, ArH), 7.33 (m, ArH), 7.22 (m, ArH), 7.20 (m, ArH), 6.82 (m, ArH), 6.80 (m, ArH), 6.18 (s, aliphatic-H), 4.16 (m, CH_2), 4.11 (m, CH_2), 3.78-3.30 (m, OCH_2), 2.49 (m, CH_2), 1.00-1.05 (m, minor aliphatic) ppm. ^{13}C NMR (100 MHz, DMSO-d_6, δ ppm): 196.326, 178.023, 159.361, 141.906, 137.306, 133.938, 129.918, 128.629, 125.141, 123.933, 120.517, 119.751, 112.137, 110.800, 73.025, 55.292, 45.829, 40.128, 39.917, 39.711, 39.500, 39.289, 39.083, 38.872. HR-MS: *m/z* found 314.0900 for $C_{17}H_{12}ClNO_3^+$.

(*Z*)-3-(2-(4-Aminophenyl)-2-oxoethylidene)-5-fluoro-indolin-2-one (3c): Creamy solid, yield 87%, m.p.: 362.78 ºC; FT-IR (KBr, ν_{max}, cm^{-1}): 3418.45 (NH *str.*), 2918.09 (sp^2-hybridized C-H *str.*), 2852.76 (sp^3-hybridized C-H *str.*), 1721.62 (>C=O) 1617.23 (>C=C<); ^{1}H NMR (400 MHz, DMSO-d_6, δ ppm): 11.09 (s, NH), 7.46 (m, ArH), 7.44 (m, ArH), 7.43 (m, ArH), 7.42 (m, ArH), 7.38 (m, ArH), 7.37 (m, ArH), 7.36 (m, ArH), 6.94 (m, ArH), 6.92 (m, ArH), 6.91 (m, ArH), 6.90 (m, ArH), 4.05 (m, CH), 3.40 (m, CH_2), 3.36 (m, CH_2), 3.15 (m, CH_2), 2.49 (m, CH_2), 2.24 (m, CH_3), 2.09 (m, CH_3), 2.00 (m, CH_3), 1.16, 1.00 (m, aliphatic); ^{13}C NMR (100 MHz, DMSO-d_6, δ ppm): 183.950, 159.433, 159.279, 156.888, 147.047, 124.647, 124.408, 118.505, 118.433, 113.584, 113.512, 111.476, 111.236, 40.128, 39.917, 39.711, 39.500, 39.294, 39.083, 38.877.

(*Z*)-5-Fluoro-3-(2-oxo-2-phenylethylidene)indolin-2-one (3d): Creamy solid, yield 88%, m.p.: 267.0 ºC; FT-IR (KBr, ν_{max}, cm^{-1}): 3141.90 (NH *str.*), 2945.02 (sp^2-hybridized C-H *str.*), 2758.04 (sp^3-hybridized C-H *str.*), 1682.43 (>C=O), 1611.63 (>C=C<). ^{1}H NMR (400 MHz, DMSO-d_6, δ ppm): 10.30 (s, NH), 7.88 (m, ArH), 7.86 (m, ArH), 7.85 (m, ArH), 7.61 (m, ArH), 7.51 (m, ArH), 7.49 (m, ArH), 7.47 (m, ArH), 7.20 (m, ArH), 7.18 (m, ArH), 6.80 (m, ArH), 6.79 (m, ArH), 6.78 (m, ArH, 6.18 (s, aliphatic-H), 4.1, 4.06 (s, CH_2), 3.6-3.15 (M, OCH_3), 2.49-2.48 (m, CH_2); ^{13}C NMR (100 MHz, DMSO-d_6, δ ppm): 196.499, 178.287, 158.973, 156.620, 139.098, 136.032, 133.617, 133.540, 133.483, 128.730, 127.896, 115.021, 114.792, 111.715, 111.471, 110.082, 110.000, 73.260, 45.690, 40.123, 39.917, 39.706, 39.500, 39.289, 39.083, 38.872.

***In silico* predictions:** The newly synthesized derivatives **3a-d** were evaluated *in silico* using the freely available web tools SwissADME and admetLAB 3.0. The physico-chemical properties such as absorption, distribution, metabolism, drug-likeness and toxicity profiles were predicted using admetLAB 3.0, which also generated radar plot visualizations. Moreover, the BOILED-Egg model in SwissADME was employed to provide key insights into the ADMET properties and drug-likeness of the synthesized compounds.

Molecular docking: Molecular docking was performed using the Glide tool in Maestro 12.8 against the target receptors, employing the extra precision (XP) method to calculate the binding energies of the ligands, which provided reliable results. Default settings included a van der Waals radius scaling factor of 0.80 Å and a partial charge cutoff of 0.15 for the non-polar parts of the ligands. After docking, the ligand-protein complexes were visualized using the pose viewer interface [25].

Ligand preparation: All chemical compounds were initially sketched in 2D using the 2D sketcher tool and uploaded to the workspace. The selected compounds were then refined by correcting bond lengths and angles through energy minimization using the OPLS_2005 force field with the LigPrep tool in Maestro 12.8. Subsequently, the Epik tool generated all possible ionization states and tautomers within a pH range of 7 ± 2 [26].

Protein preparation and grid generation: The crystal structures of targeted proteins retrieved from the Protein Data Bank (https://www.rcsb.org/) with PDB IDs 9GZH and 4ASD, having resolution of 2.2 Å and 2.03 Å, respectively. Before docking, all the heteroatoms and water molecules were removed and missing hydrogens were added to the proteins. Afterward, zero-bond order disulfide bonds converted the selenomethionines into methionines, filling the missing side chains and loops and pre-processing the proteins using the protein preparation wizard tool (Maestro 12.8). Moreover, all the altered hydrogens were optimized at 7.0 pH using the PROPKA tool. At the end, the proteins were minimized by the OPLS_2005 force field and converged heavy atoms below 0.30 Å. Subsequently, the active sites of proteins were found by choosing the native ligands and generating the grids over the active sites -53.07, -2.21, 11.09 and -26.73, -1.92, -10.79 coordinates, respectively. Furthermore, the van der Waal radius 1.0 Å and 0.25 partial charges cut-off scaling factor was set for non-polar parts of the receptor [27].

RESULTS AND DISCUSSION

In silico predictions

Physico-chemical properties: The physico-chemical profiling of the synthesized compounds **3a-d** (calculated *via* AdmetLab3.0 showed acceptable values for drug-like molecular weight, 267.07-357.0 Da. While molecular weight values suggested the potential for oral bioavailability per Lipinski's rule of five, calculated densities and molecular volumes quantified a relatively small size for the molecules and the number of hydrogen bond acceptors (nHA = 3-4) and donors (nHD = 1-3) were below their limits pertaining to biological target binding. The flexibility index and the number of rotatable bonds (2-3) suggested a helpful balance of rigidity in a molecular structure that is relevant to receptor binding affinity. The LogP values of 2.1-3.3 suggesting moderate lipophilicity were consistent with logD 7.4 values near an acceptable value of 3. The pre-

dicted melting and boiling points confirmed thermal stability and the pK_a values confirmed potentials for ionization under physiological conditions (Table-1).

Absorption: The absorption profiles of the synthesized compounds **3a-d** showed variable permeability across models. The Caco-2 permeability values indicated potential moderate intestinal absorption, while the MDCK permeability was negligible, implying limited passive diffusion across renal epithelial cells. The PAMPA results were mostly negative, indicating low passive permeability. Compounds **3a**, **3b** and **3d** had strong P-glycoprotein (Pgp) inhibition (+++), which may confer a pathway for drug resistance associated with efflux, often a major constraint in cancer and antimicrobial therapy. Human intestinal absorption (HIA) values were relatively weak, indicating that while lipophilicity was favourable, intestinal uptake may be limited and likely needed a formulative strategy to increase bioavailability. Overall, the absorption profile showed moderate permeability with possible benefits from Pgp inhibition. The following symbols represents the following values: 0-0.1 (---), 0.1-0.3 (--), 0.3-0.5 (-), 0.5-0.7 (+), 0.7-0.9 (++) and 0.9-1.0 (+++) (Table-2).

Distribution: The distribution parameters of the synthesized compounds **3a-d** indicated significant plasma protein binding from 91.1% to 98.9%, showing a high affinity for plasma proteins and the potential for prolonged circulation half-life. Compounds **3a** and **3c** had higher steady-state volumes of distribution (VDss), implying greater tissue distribution and penetration than **3b** and **3d** compounds. None of the derivatives indicated blood-brain barrier penetration, directing minimal concerns with central nervous system (CNS)-related side effects, which could favour a positive for peripheral disease-oriented investigations. The inhibitory predictions demonstrated strong inhibitory potential with hepatic transporters OATP1B1 and OATP1B3 in compounds **3a** and **3b**, which represents potential drug-drug interaction. While the lack of BCRP and MRP1 inhibition lessens the concerns for efflux-related clearance, the universal inhibition of BSEP would raise concerns for cholestasis-related toxicities. Based on the profile of the distribution potential, this presents a positive balance for plasma retention and tissue distribution and penetration. The following symbols represents the following values: 0-0.1 (---), 0.1-0.3 (--), 0.3-0.5 (-), 0.5-0.7 (+), 0.7-0.9 (++) and 0.9-1.0 (+++) (Table-3).

Metabolism: Interaction studies involving CYP enzymes indicated that all the compounds **3a-d** are potent inhibitors of CYP1A2, CYP2C19, CYP2C9, CYP3A4 and CYP2C8, which may present large metabolic drug-drug interactions. Among these, compounds **3a** and **3b** were observed to be more broad-spectrum inhibitors while compound **3c** was relatively weaker. The results of substrate prediction suggested little metabo-

TABLE-1
PHYSICO-CHEMICAL PROPERTIES OF SYNTHESIZED COMPOUNDS **3a-d**

Parameters	**3a**	**3b**	**3c**	**3d**	Sunitinib
Molecular weight	357.0	313.05	282.08	267.07	398.21
Volume	309.842	305.769	281.536	270.539	409.942
Density	1.152	1.024	1.002	0.987	0.971
nHA	4.0	4.0	4.0	3.0	6.0
nHD	1.0	1.0	3.0	1.0	3.0
nRot	3.0	3.0	2.0	2.0	8.0
nRing	3.0	3.0	3.0	3.0	3.0
MaxRing	9.0	9.0	9.0	9.0	9.0
nHet	5.0	5.0	5.0	4.0	7.0
fChar	0.0	0.0	0.0	0.0	0.0
nRig	19.0	19.0	19.0	19.0	18.0
Flexibility	0.158	0.158	0.105	0.105	0.444
Stereo centers	0.0	0.0	0.0	0.0	0.0
TPSA	55.4	55.4	72.19	46.17	77.23
logS	-4.702	-4.778	-3.881	-4.325	-4.12
logP	3.302	3.316	2.167	2.968	3.018
logD7.4	3.186	3.201	2.257	3.0	2.808
pka (acid)	9.607	9.497	8.989	9.204	10.001
pka (base)	4.004	4.124	2.952	3.197	7.238
Melting point	187.496	180.615	220.371	220.902	177.363
Boiling point	344.648	343.262	350.94	353.888	325.763

TABLE-2
DETAILS OF DRUGLIKENESS OF SYNTHESIZED COMPOUNDS **3a-d**

Parameters	**3a**	**3b**	**3c**	**3d**	Sunitinib
Caco-2 permeability	-4.852	-4.722	-5.091	-4.777	-5.566
MDCK permeability	0.0	0.0	0.0	0.0	0.0
PAMPA	---	---	--	---	---
Pgp inhibitor	+++	+++	-	+++	+++
Pgp substrate	---	---	---	---	---
HIA	--	---	---	---	---

TABLE-3
DETAILS OF INHIBITORY EFFECT OF COMPOUNDS **3a-d**

Parameters	**3a**	**3b**	**3c**	**3d**	Sunitinib
PPB	98.1%	98.9%	91.1%	97.5%	87.0%
VDss	1.504	0.385	1.257	0.849	3.297
BBB	---	---	---	---	---
Fu	1.9%	0.6%	8.8%	2.4%	11.3%
OATP1B1 inhibitor	+++	+++	-	+	-
OATP1B3 inhibitor	+++	+++	+	++	--
BCRP inhibitor	---	---	---	---	---
MRP1 inhibitor	---	---	---	---	--
BSEP inhibitor	+++	+++	+++	+++	+++

lism through CYP pathways, which would cause a larger half-life and systemic persistence. Human liver microsome (HLM) half-life results indicated low-to-moderate stability for particularly compounds **3a** and **3d**. The following symbols represents the following values: 0-0.1 (---), 0.1-0.3 (--), 0.3-0.5 (-), 0.5-0.7 (+), 0.7-0.9 (++) and 0.9-1.0 (+++) (Table-4).

Medicinal chemistry: Medicinal chemistry assessments of the synthesized compounds **3a-d** indicated favourable drug likeness characteristics across the compounds. The quantitative estimate of drug-likeness (QED) values were in the range of 0.505 to 0.696 in compound **3b**, indicating its favourable drug-likeness properties. The synthetic accessibility (SAscore) and general accessibility (GASA) values of the compounds indicate that they would be relatively straightforward to synthesise the target compounds, which is desirable for those intending to develop compounds on a larger scale. The Lipinski, GSK and Golden Triangle rules were fulfilled for all derivatives, demonstrating potential drug-like properties (Table-5). While two derivatives **3a** and **3b** were rejected for potential liabilities according to Pfizer's rule and none of the derivatives triggered PAINS or BMS alerts, suggesting a lower possibility of observing false-positive bioactivities. Although the results from the colloidal aggregation and fluorescence assays indicated potential issues, they suggest that careful precautions should be taken when conducting biological screening with these derivatives.

Toxicophore rules: Toxicophore-based evaluations of the synthesized compounds **3a-d** demonstrated that all compounds satisfied the filters associated with major drug safety with no or minor alerts associated with acute toxicity or carcinogenicity. Given that all predictions of mutagenicity were low and compounds **3c** showed marginally increased risk compared to the other compounds. In general, alerts for skin sensitization were similar across all derivatives indicating a common feature of structure responsible for inducing a mild sensory assessment. Predictions for compounds **3b-d** demonstrated little biodegradability for concern about exposure for bioaccumulation and persistence in the environment (Table-6). Importantly all compounds had favourable Sure ChEMBL and FAF-Drugs 4, indicating suitable safety margins.

Toxicity: Toxicity assessment found variable risk profiles among the compounds **3a-d**. Assessment of hERG inhibition found moderate values indicating some risk of cardiovascular toxicity, particularly for compound **3b**. Drug-induced liver injury (DILI) concerns were prevalent in all the derivatives, indicating the need to carefully observe hepatotoxicity. The predictions for Ames mutagenicity found that all derivatives exhibit some mutagenic propensity, while compound **3c** exhibiting the highest mutagenic potential in accordance with the genotoxicophore alert. Predictive toxicity for human hepatotoxicity, nephrotoxicity and neurotoxicity was generally high in the series, with compounds **3c** and **3d** placing higher in human hepatotoxicity and nephrotoxicity. With the noted potential to penetrate the blood-brain barrier, neurotoxicity regarding compounds **3c** and **3d** becomes more clinically relevant due to the increased chance for central effects (Table-7). Conver-

TABLE-4
DETAILS OF METABOLISM OF COMPOUNDS **3a-d**

Parameters	**3a**	**3b**	**3c**	**3d**	Sunitinib
CYP1A2 inhibitor	+++	+++	++	+++	-
CYP1A2 substrate	-	-	---	---	--
CYP2C19 inhibitor	+++	+++	--	++	---
CYP2C19 substrate	---	---	---	---	-
CYP2C9 inhibitor	+++	+++	-	+++	---
CYP2C9 substrate	---	---	---	---	---
CYP2D6 inhibitor	--	---	---	---	---
CYP2D6 substrate	---	---	---	---	---
CYP3A4 inhibitor	+++	+++	+++	+	---
CYP3A4 substrate	++	++	-	+	+
CYP2B6 inhibitor	++	+++	++	---	---
CYP2B6 substrate	---	---	---	---	---
CYP2C8 inhibitor	+++	++	+++	+++	---
HLM Stability	--	-	---	--	---

TABLE-5
DETAILS OF DRUGLIKENESS EFFECTS OF COMPOUNDS **3a-d**

Parameters	**3a**	**3b**	**3c**	**3d**	Sunitinib
QED	0.673	0.696	0.505	0.671	0.626
SAscore	Easy	Easy	Easy	Easy	Easy
GASA	Easy	Easy	Easy	Easy	Easy
Fsp^3	0.059	0.059	0.0	0.0	0.364
MCE-18	34.0	34.0	34.0	32.0	40.0
NPscore	-0.519	-0.652	-0.742	-0.809	-1.208
Lipinski rule	Accepted	Accepted	Accepted	Accepted	Accepted
Pfizer rule	Rejected	Rejected	Accepted	Accepted	Accepted
GSK rule	Accepted	Accepted	Accepted	Accepted	Accepted
GoldenTriangle	Accepted	Accepted	Accepted	Accepted	Accepted
PAINS	0	0	0	0	0
Alarm_NMR rule	4	3	3	2	1
BMS rule	0	0	0	0	0
Chelating rule	0	0	0	0	0
Colloidal aggregators	0.957	0.949	0.924	0.799	0.347
FLuc inhibitors	0.848	0.858	0.974	0.919	0.525
Blue fluorescence	0.268	0.437	0.384	0.314	0.37
Green fluorescence	0.903	0.915	0.635	0.735	0.596
Reactive compounds	0.019	0.019	0.058	0.043	0.001
Promiscuous compounds	0.233	0.489	0.301	0.304	0.91

TABLE-6
DETAILS OF TOXICOPHORE EFFECTS OF COMPOUNDS **3a-d**

Parameters	**3a**	**3b**	**3c**	**3d**	Sunitinib
Aquatic toxicity rule	4	4	4	4	4
Genotoxic carcinogenicity mutagenicity rule	2	2	6	2	1
Nongenotoxic carcinogenicity rule	2	2	2	2	1
Skin sensitization rule	5	5	5	5	5
Acute toxicity rule	0	0	0	0	0
Nonbiodegradable	0	1	1	1	2
SureChEMBL rule	0	0	0	0	0
FAF-Drugs4 rule	2	2	3	2	3

TABLE-7
DETAILS OF TOXIC NATURE OF COMPOUNDS **3a-d**

Parameters	**3a**	**3b**	**3c**	**3d**	Sunitinib
hERG blockers	0.17	0.247	0.097	0.155	0.888
hERG blockers (10 μm)	0.719	0.779	0.622	0.768	0.868
DILI	0.984	0.983	0.971	0.987	0.96
AMES toxicity	0.461	0.507	0.875	0.621	0.933
Rat oral acute toxicity	0.555	0.472	0.665	0.498	0.88
FDAMDD	0.821	0.691	0.636	0.723	0.987
Skin sensitization	0.916	0.885	0.874	0.955	0.999
Carcinogenicity	0.63	0.587	0.724	0.503	0.658
Eye corrosion	0.031	0.015	0.008	0.018	0.0
Eye irritation	0.994	0.981	0.995	0.996	0.006
Respiratory	0.451	0.419	0.893	0.749	0.992
Human hepatotoxicity	0.971	0.978	0.977	0.996	0.993
Drug-induced nephrotoxicity	0.446	0.686	0.828	0.829	0.994
Drug-induced neurotoxicity	0.754	0.793	0.961	0.716	0.986
Ototoxicity	0.282	0.399	0.458	0.33	0.92
Hematotoxicity	0.759	0.849	0.866	0.747	0.966
Genotoxicity	0.977	0.919	0.999	0.99	1.0
RPMI-8226 immunitoxicity	0.027	0.027	0.021	0.015	0.191
A549 cytotoxicity	0.024	0.05	0.012	0.015	0.421
Hek293 cytotoxicity	0.48	0.662	0.494	0.37	0.858
BCF	1.577	1.509	1.17	1.354	1.051
IGC50	4.639	4.623	3.823	4.046	3.462
LC50DM	6.086	6.035	5.242	5.521	4.996
LC50FM	5.66	5.601	4.415	4.913	4.409

sely, predicted *in vitro* cytotoxicity in RPMI-8226, A549 and HEK293 cells were low-moderate toxicity supporting selective safety.

TOX21 pathway: The Tox21 pathway analysis of the compounds **3a-d** indicated that compounds activated NR-AhR, SR-ARE, SR-MMP and SR-p53 pathways, all of which are associated with oxidative stress responses, metabolic regulation and apoptosis induction. These properties might represent potential anticancer or chemopreventive applications and there was minimal activation of androgen, estrogen and PPAR-γ receptors, therefore endocrine disruption was not a concern. Certainly, there is an opportunity for neuro-oncological therapeutics, but there is also potential for neurotoxicity, considering the probability of BBB crossing and the potential for activating oxidative stress and apoptosis in the CNS. The following symbols represents the following values: 0-0.1 (---), 0.1-0.3 (--), 0.3-0.5 (-), 0.5-0.7 (+), 0.7-0.9 (++) and 0.9-1.0 (+++) (Table-8).

Radar view: The radar plots visualized the balance of the physico-chemical, pharmacokinetic and safety properties of the synthesized derivatives relative to FDA approved drugs. Compounds **3a** and **3b** had overlaps with the reference space of approved drugs meaning they may have some desirable drug-like properties, while compound **3c** was separated from the other compounds due to undesirable properties (Fig. 1).

Boiled egg: The SwissADME Boiled Egg model indicated a strong likelihood for the synthesized compounds **3a-d** to penetrate the BBB, showing all of the derivatives were in the yellow zone suggesting BBB transport, which could open these compounds up to CNS therapeutics while also raising issues of non-target CNS exposure (Fig. 2).

Molecular docking: All the screened synthesized compounds (**3a-d**) exhibited binding affinities in the range of –11.633 to –11.973 kcal/mol toward the 9GZH protein in molecular docking studies (Table-9). Among the compounds, **3b** compound was calculated with the -11.973 kcal/mol lowest binding energy that indicated the hydrogen bond to Cys677 and eighteen hydrophobic interactions (Fig. 3). Similarly, the molecular docking was executed against 4ASD and calculated the binding energy -6.678 – -7.726 kcal/mol (Table-10) and found that compound **3d** deliberated the -7.726 kcal/mol against 4ASD and established hydrogen bond to Val914, Asp1046 amino acids along with fifteen hydrophobic interactions (Fig. 4). On the other hand, the control drug (sunitinib) was estimated at -8.993 kcal/mol and -5.759 kcal/mol against 9GZH and 4ASD. Furthermore, sunitinib indicated a hydrogen bond to Cys677 with nineteen hydrophobic interactions for 9GZH, but the sunitinib formed a hydrogen bond to Cys919 and π-cation contact to Lys868 along with nineteen hydrophobic interactions. During the molecular docking, the

TABLE-8
DETAILS OF TOX21 PATHWAY NATURE OF COMPOUNDS **3a-d**

Parameters	**3a**	**3b**	**3c**	**3d**	Sunitinib
NR-AhR	+++	+++	++	++	---
NR-AR	---	---	---	---	---
NR-AR-LBD	---	---	--	--	---
NR-Aromatase	--	--	-	--	---
NR-ER	--	--	--	---	-
NR-ER-LBD	---	---	---	---	---
NR-PPAR-gamma	---	---	--	--	---
SR-ARE	+++	+++	+++	+++	+
SR-ATAD5	---	---	--	---	---
SR-HSE	+++	+++	++	+++	---
SR-MMP	+++	+++	+++	+++	---
SR-p53	+++	+++	++	+++	--

TABLE-9
THE BINDING ENERGY OF COMPOUNDS **3a-d** AND STANDARD DRUG (SUNITINIB) AGAINST PDGFRα

Compound	Binding energy (9GZH)	Interactions
3a	-11.970	**H-bond:** Cys677 **Hydrophobic:** Leu599, Val607, Ala625, Val626, Lys627, Glu644, Met648, Val658, Ile672, Ile674, Glu675, Tyr676, Gly680, Asp681, Leu825, Cys835, Asp836, Phe837
3b	-11.973	**H-bond:** Cys677 **Hydrophobic:** Leu599, Val607, Ala625, Val626, Lys627, Glu644, Met648, Val658, Ile672, Ile674, Glu675, Tyr676, Gly680, Asp681, Leu825, Cys835, Asp836, Phe837
3c	-11.633	**H-bond:** Cys677, Glu644 **Hydrophobic:** Leu599, Val607, Ala625, Val626, Lys627, Met648, Val658, Ile672, Ile674, Glu675, Tyr676, Gly680, Asp681, Leu825, Cys835, Asp836, Phe837
3d	-11.852	**H-bond:** Cys677 **Hydrophobic:** Leu599, Val607, Ala625, Val626, Lys627, Glu644, Met648, Val658, Ile672, Ile674, Glu675, Tyr676, Gly680, Leu825, Cys835, Asp836, Phe837
Sunitinib	-8.993	**H-bond:** Cys677 **Hydrophobic:** Leu599, Val607, Ala625, Val626, Lys627, Glu644, Met648, Leu651, Ile657, Val658, Ile674, Tyr676, Gly680, Asp681, Leu825, Ile834, Cys835, Asp836, Phe837

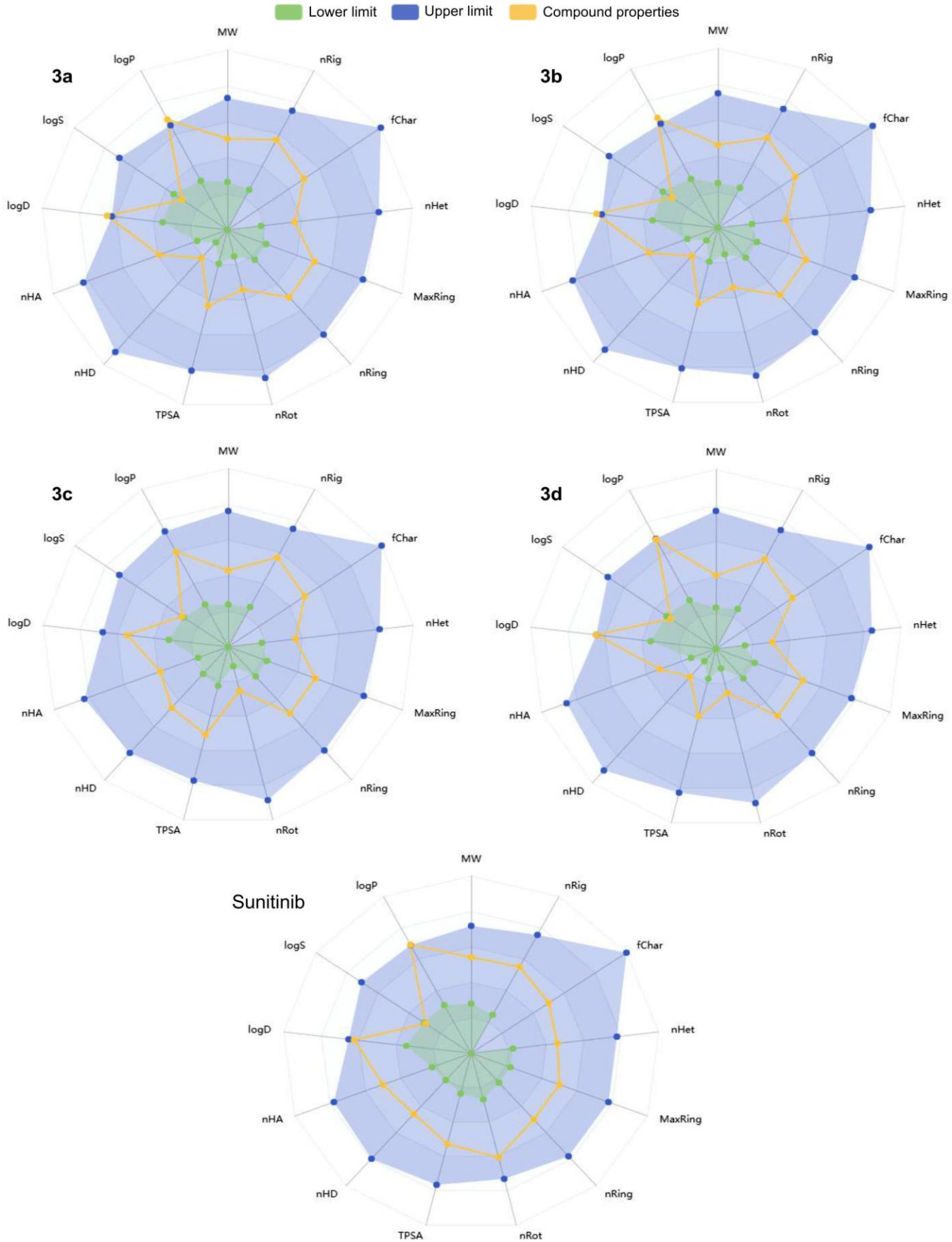

Fig. 1. A view of radar detailing for synthesized compounds and FDA approved drug (sunitinib)

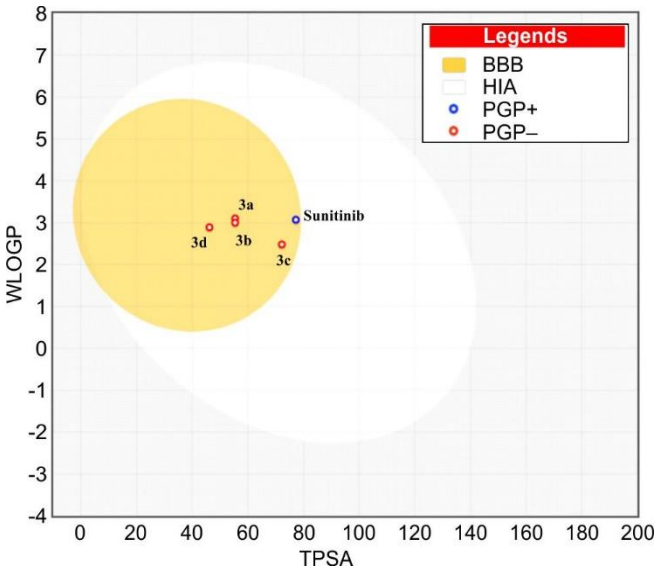

Fig. 2. Boiled egg of the synthesized derivatives **3a-d** and standard drug (sunitinib)

docking pose of both ligand-protein complexes was analyzed and demonstrated the highly stable in the active site of protein; compounds **3b** and **3d** indicated the hydrogen bonds with Cys677, Asp1046 and Val914 amino acids that are responsible for causing disease [28]. Therefore, the docked complexes demonstrated significant binding affinities between the synthesized oxindole–chalcone derivatives (as ligands) and the PDGFRα and VEGFR2 proteins. PDGFRα and VEGFR2 are two closely related receptor tyrosine kinases *viz.* PDGFRα and VEGFR2 that play pivotal roles in regulating cell proliferation, survival and angiogenesis. Dysregulation of these receptors is frequently associated with the progression of various cancers. Hence, the strong binding affinities observed in the docking studies suggest the potential of oxindole–chalcone derivatives as promising dual inhibitors targeting PDGFRα and VEGFR2.

Conclusions

In this study, oxindole-containing chalcone derivatives **3a-d** were successfully synthesized and their structures were

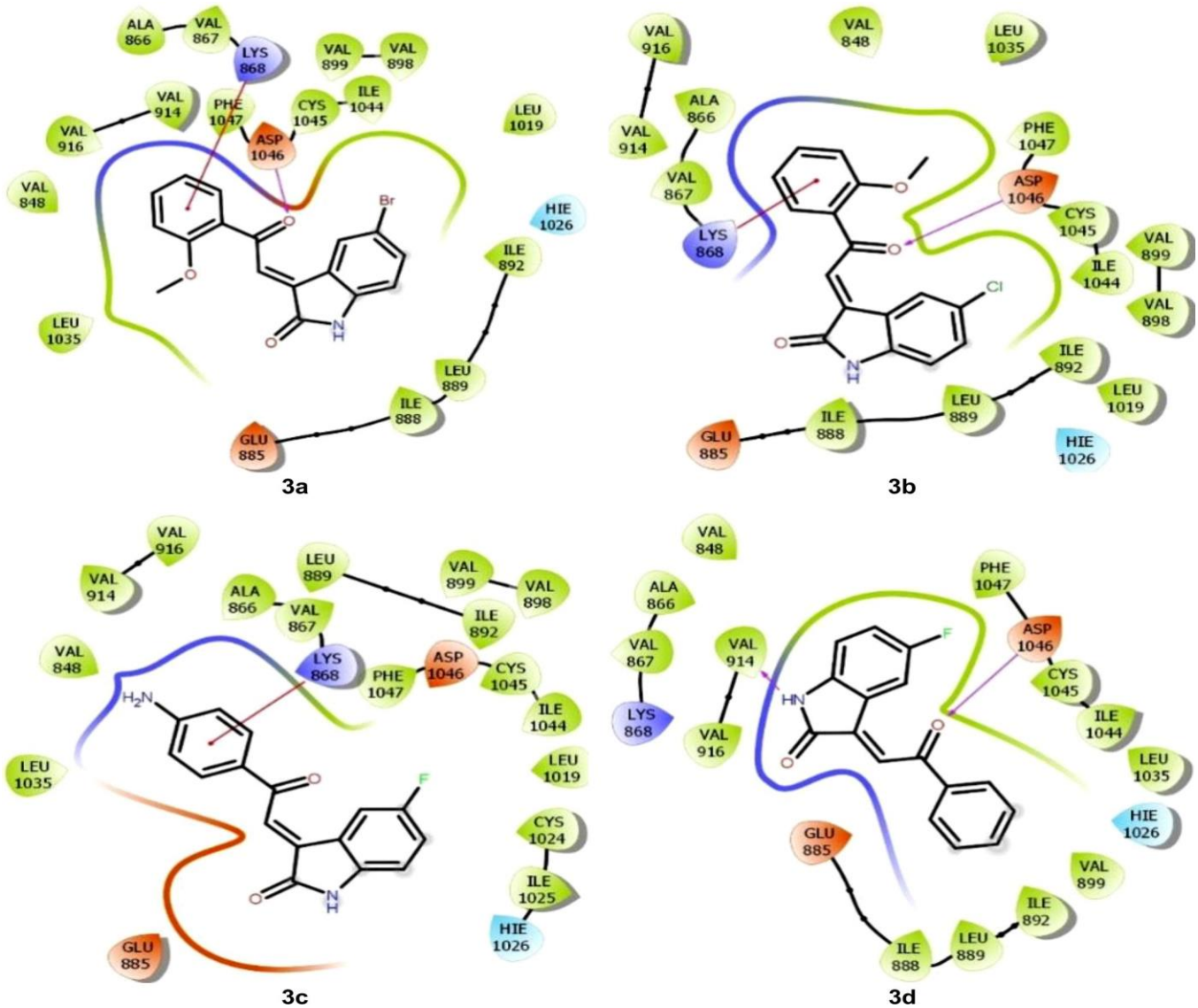

Fig. 3. Predicted binding patterns of VEGFR2 inhibitors (**3a-d**)

TABLE-10
THE BINDING ENERGY OF COMPOUNDS **3a-d** AND STANDARD DRUG (SUNITINIB) AGAINST VEGFR2

Compound	Binding energy (9GZH)	Interactions
3a	-7.247	**H-bond:** Asp1046 **π-cation:** Lys868 **Hydrophobic:** Val848, Ala866, Val867, Glu885, Ile888, Leu889, Ile892, Val898, Val899, Val914, Val916, Leu1019, Hie1026, Leu1035, Ile1044, Cys1045, Phe1047
3b	-7.530	**H-bond:** Asp1046 **π-cation:** Lys868 **Hydrophobic:** Val848, Ala866, Val867, Glu885, Ile888, Leu889, Ile892, Val898, Val899, Val914, Val916, Hie1026, Leu1035, Ile1044, Cys1045, Phe1047
3c	-6.678	**π-cation:** Lys868 **Hydrophobic:** Val848, Ala866, Val867, Glu885, Leu889, Ile892, Val898, Val899, Val914, Val916, Leu1019, Cys1024, Ile1025, Hie1026, Leu1035, Ile1044, Cys1045, Asp1046, Phe1047
3d	-7.726	**H-bond:** Val914, Asp1046 **Hydrophobic:** Val848, Ala866, Val867, Lys868, Ile888, Leu889, Ile892, Val899, Val916, Glu885, Hie1026, Leu1035, Ile1044, Cys1045, Phe1047
Sunitinib	-5.759	**H-bond:** Cys919 **π-cation:** Lys868 **Hydrophobic:** Lys838, Leu840, Val848, Glu850, Ala866, Val867, Glu885, Leu889, Val899, Val914, Val916, Glu917, Phe918, Lys920, Phe921, Gly922, Leu1035, Cys1045, Phe1047

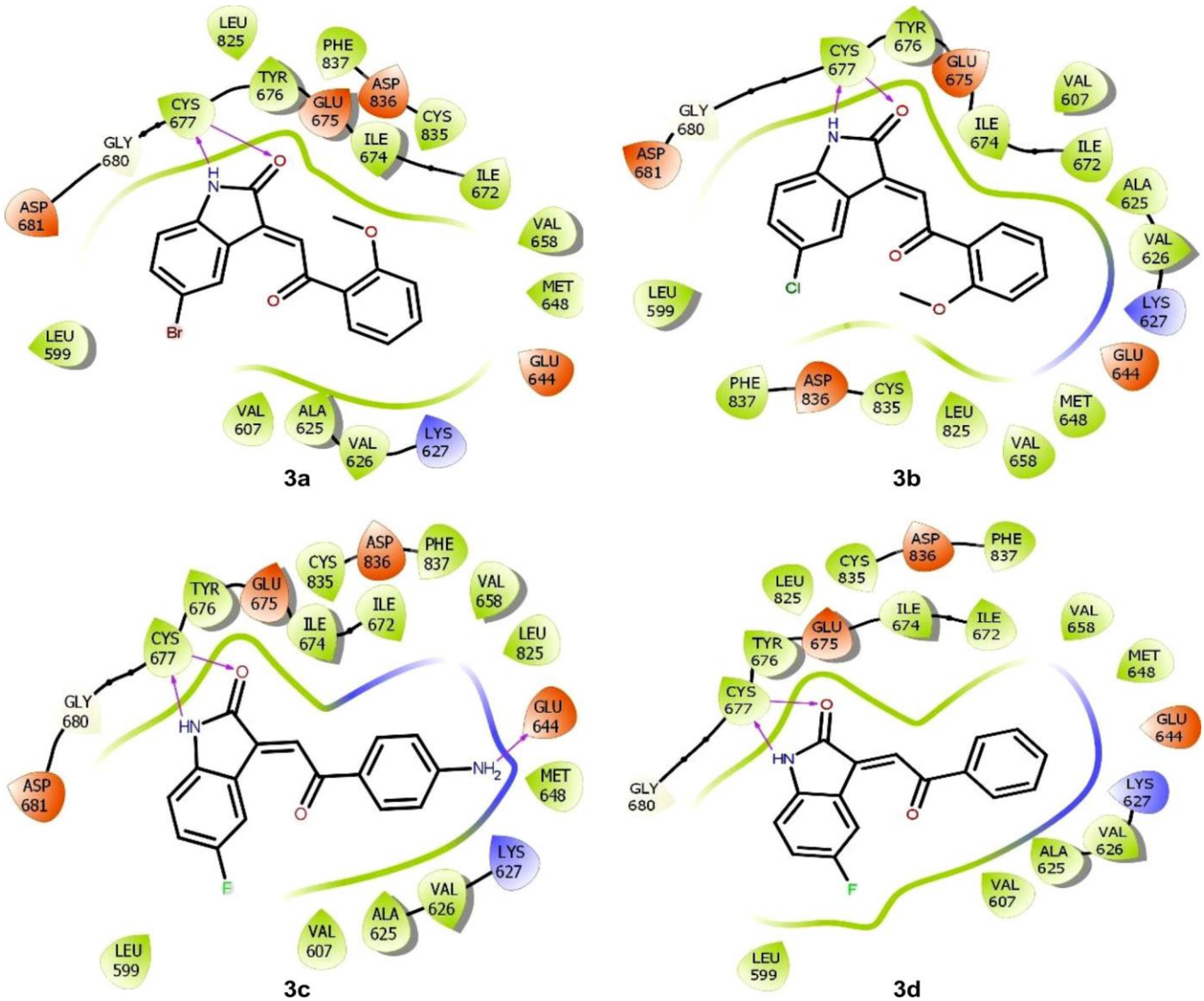

Fig. 4. Predicted binding patterns of PDGFRα inhibitors (**3a-d**)

confirmed through IR, NMR and HRMS spectral techniques. The *in silico* analysis showed that these compounds have drug-like properties, pharmacokinetic profiles and safety profiles to support their development as anticancer candidate. All the synthesized compounds were synthesized and investigated their biological significance as preliminary analysis under ADMET/ molecular docking. The molecular docking studies further demonstrated that compounds **3a-d** have high theoretical bin ding affinities and stable interactions compared to standard drug sunitinib with the protein target like PDGFRα (PDB ID: 9GZH) and VEGFR2. Overall, these studies show that poly-functional oxindole-chalcone hybrids could be explored further as lead molecules in anticancer therapeutic applications.

ACKNOWLEDGEMENTS

The authors gratefully acknowledge the Research and Development Division, Integral University, Lucknow, India, for assigning the Manuscript Communication No. (MCN: IU/ R&D/2025-MCN0003886) and for providing the facilities required to conduct this research.

CONFLICT OF INTEREST

The authors declare that there is no conflict of interests regarding the publication of this article.

REFERENCES

1. Y.S. Quan, J.Y. Liu, Y.L. Wang, Z. Liu, Z.S. Quan, S.H. Wang and X.M. Yin, *Chem. Biodivers.*, **22**, e202401953 (2025); https://doi.org/10.1002/cbdv.202401953
2. M. Abdelaziz, H.A. Abou-Zied, E.A. Beshr and A.M. Hayallah, *J. Adv. Biomed. Pharm. Sci.*, **6,** 90 (2023); https://doi.org/10.21608/jabps.2023.184496.1177
3. K. Mezgebe, Y. Melaku and E. Mulugeta, *ACS Omega*, **8**, 22, 19194 (2023); https://doi.org/10.1021/acsomega.3c01035
4. S.K. Suthar, S. Bansal, N. Narkhede, M. Guleria, A.T. Alex and A. Joseph, *Chem. Pharm. Bull.*, **65**, 833 (2017); https://doi.org/10.1248/cpb.c17-00301
5. D. Karati, *Discover Chemistry*, **1**, 66 (2024); https://doi.org/10.1007/s44371-024-00073-z
6. S. Bugalia, Y. Dhayal, H. Sachdeva, S. Kumari, K. Atal, U. Phageria, P. Saini, and O. P. Gurjar, *J. Inorg. Organomet. Polym.*, **33**, 1782 (2023); https://doi.org/10.1007/s10904-023-02666-0
7. C. Shekhar Yadav, I. Azad, A. Rahman Khan, M. Nasibullah, N. Ahmad, D. Hansda, S. Nusrat Ali, K. Shrivastav, M. Akil and M.B. Lohani, *Results Chem.*, **7**, 101326 (2024); https://doi.org/10.1016/j.rechem.2024.101326
8. E.N. Okolo, D.I. Ugwu, B.E. Ezema, J.C. Ndefo, F.U. Eze, C.G. Ezema, J.A. Ezugwu and O.T. Ujam, *Sci. Rep.*, **11**, 21781 (2021); https://doi.org/10.1038/s41598-021-01292-5
9. S.N. Ali, C.S. Yadav, M.A. Khan, A. Kamal, A.R. Khan, I. Azad et al., *Am. J. Psychiatr. Rehabil.*, **28**, 346 (2025); https://doi.org/10.69980/ajpr.v28i1.97
10. F. Hassan, I. Azad, M. Asif, D. Shukla, A. Husain, A.R. Khan, M. Saquib and M. Nasibullah, *Med. Chem.*, **19**, 413 (2023); https://doi.org/10.2174/1573406418666220930145336
11. Y. Ouyang, J. Li, X. Chen, X. Fu, S. Sun and Q. Wu, *Biomolecules*, **11**, 894 (2021); https://doi.org/10.3390/biom11060894
12. M.A. Alshams, M.S. Nafie, H.F. Ashour and A.S.A. Yassen, *RSC Adv.*, **15**, 32188 (2025); https://doi.org/10.1039/D5RA05002B
13. C.S. Yadav, I. Azad, A.R. Khan, N. Ahmad, S.K. Gupta, V.K. Verma, D. Hansda and M.B. Lohani, *Curr. Bioact. Compd.*, **20**, 12 (2024); https://doi.org/10.2174/0115734072266590231023094928
14. A. Mittal, V.K. Vashistha and D.K. Das, *Free Radic. Res.*, **56**, 378 (2022); https://doi.org/10.1080/10715762.2022.2120396
15. A. Yadav, V. Sharma and G. Singh, *ChemistrySelect*, **9**, e202401321 (2024); https://doi.org/10.1002/slct.202401321
16. J. Syahri, R. Hilma, A.H. Ali, N. Ismail, N. Yee Ling, Nurlaili, B.A. Nurohmah, H.K. Agustar, L.Y. Ling and J. Latip, *RSC Advances*, **13**, 36035 (2023); https://doi.org/10.1039/D3RA05361J
17. D. Elkhalifa, I. Al-Hashimi, A.E. Al Moustafa and A. Khalil, *J. Drug Target.*, **29**, 403 (2021); https://doi.org/10.1080/1061186X.2020.1853759
18. R.E. Ferraz de Paiva, E.G. Vieira, D. Rodrigues da Silva, C.A. Wegermann and A.M. Costa Ferreira, *Front. Mol. Biosci.*, **7**, 627272 (2021); https://doi.org/10.3389/fmolb.2020.627272
19. R. Nath, S. Pathania, G. Grover and M.J. Akhtar, *J. Mol. Struct.*, **1222**, 128900 (2020); https://doi.org/10.1016/j.molstruc.2020.128900
20. R. Swati, A. Raza, S. Chowdhary, A. Anand, Shaveta, A.K. Sharma, K. Kumar and V. Kumar, *ChemMedChem*, **19**, e202400015 (2024); https://doi.org/10.1002/cmdc.202400015
21. S. Kumar, J.M. Oh, P. Prabhakaran, A. Awasti, H. Kim and B. Mathew, *Sci. Rep.*, **14**, 1264 (2024); https://doi.org/10.1038/s41598-024-51728-x
22. V.K.R. Tangadanchu, Y.F. Sui and C.H. Zhou, *Bioorg. Med. Chem. Lett.*, **41**, 128030 (2021); https://doi.org/10.1016/j.bmcl.2021.128030
23. D. Mukherji, J. Larkin and L. Pickering, *Fut. Oncol.*, **6**, 1377 (2010); https://doi.org/10.2217/fon.10.94
24. I. Azad, M. Nasibullah, T. Khan, F. Hassan and Y. Akhter, *J. Mol. Graph. Model.*, **81**, 211 (2018); https://doi.org/10.1016/j.jmgm.2018.02.013
25. V. Varun, S. Sonam and R. Kakkar, *MedChemComm*, **10**, 351 (2019); https://doi.org/10.1039/C8MD00585K
26. W.A. Ansari, M.A. Khan, F. Rizvi, K. Ali, M.K. Hussain, M. Saquib and M.F. Khan, *Future Pharmacol.*, **2**, 558 (2022); https://doi.org/10.3390/futurepharmacol2040034
27. A.R. Pandey, W.A. Ansari, P. Maurya, H. Aslam, R.R. Pandey, D.P. Mishra, S.O. Rab, S. Ahmad, P. Puri and M.F. Khan, *ChemistrySelect*, **10**, e202500637 (2025); https://doi.org/10.1002/slct.202500637
28. W.A. Ansari, S.O. Rab, M. Saquib, A. Sarfraz, M.K. Hussain, M.S. Akhtar, I. Ahmad and M.F. Khan, *Molecules*, **28**, 5853 (2023); https://doi.org/10.3390/molecules28155853